Additively Manufactured Cryogenic Microchannel Distillation Device for Air Separation

Danny Bottenus[1], Paul Humble[1], Russell Burnett[1], Warren Harper[1], Tim Veldman[2], Michael Powell[1], John Barclay[1], and James Ely[1]

[1]Pacific Northwest National Laboratory
[2]WhiteSpace Engineering LLC

March 31, 2022

Abstract

The efficiency of air separation is tested using three different small scale cryogenic distillation columns. The performance of a random packed column is compared to the performance of two microchannel distillation (MCD) columns that use thin wicking structures and gas flow channels to achieve process intensification. The MCD columns tested include a plate-type layered (PTL) column and an additively manufactured porous honeycomb (AMPH) column. For columns with 25.4 cm of active height and run under similar conditions, the packed, PTL, and AMPH columns achieved approximate height equivalent of a theoretical plate (HETP) values of 5.5, 3.7, and 3.2 cm for nitrogen, and 5.9, 4.9, and 3.3 cm for argon. The AMPH column can produce up to 0.4 SLM of 90+% purity oxygen with 12 W of cooling lift. These results demonstrate the feasibility of using additive manufacturing to construct MCD devices and pave a way for constructing novel MCD designs.

Introduction

Air separation refers to the process of separating air into its primary components. The motivation is usually to provide concentrated streams of oxygen and nitrogen. In some cases, the recovery of argon and other noble gases is of interest. For example, there is an increasing interest in developing air separation processes to collect xenon from the atmosphere for large-scale physics experiments.[1] Air separation processes are also a vital part of radioxenon monitoring systems used in the International Monitoring System for detecting nuclear explosions.[2] The work presented here is motivated by the desire to develop small energy-efficient air separation equipment that can be used to produce pure gasses from the atmosphere including oxygen, nitrogen, argon, and xenon.

A variety of processes are currently used for air separation, including cryogenic distillation, temperature and/or pressure swing adsorption, and membrane separation.[3-7] Adsorption and membrane-based processes are often used at smaller scales but are generally less energy efficient than large cryogenic distillation plants used for large-scale production. Here we explore the miniaturization of cryogenic distillation to provide a small energy-efficient air separation method that favorably competes with other small-scale air separation processes and systems. Importantly, distillation is a versatile process that can be tuned for the collection and purification of various gas species present in air, as well as other separations important to industry.

A traditional distillation column contains a series of horizontal trays spaced at regular intervals along the column. These trays provide regions for the liquid to pool and contact the vapor phase, with more-volatile components becoming concentrated in the vapor and less-volatile ones becoming concentrated in the liquid.

Alternatively, the trays can be replaced with packing material of various shapes and sizes, with vapor-liquid contact occurring more regularly along the column, rather than only at trayed intervals.

A fundamental concept in distillation columns is the ideal stage. This is the separation that is achieved when a vapor and liquid are contacted and the components in these phases are allowed to partition and come to equilibrium. The trays in a trayed column allow for vapor liquid contact; however, imperfect mixing and mass transfer constraints may prevent full equilibrium from being reached on each tray. Thus, the separation achieved in a trayed distillation column is lower than that expected if each tray was an equilibrium stage. One measure of efficiency (η) in a trayed column is:

$\eta = \frac{N_{\text{stages}}}{N_{\text{trays}}}$ (1)

where N_{stages} is the number of ideal stages required to achieve the measured separation, and N_{trays} is the actual number of column trays.

In packed columns, the lack of physical trays requires a different metric for efficiency. A frequently used performance metric is the height equivalent of a theoretical plate ($HETP$), or the length of packing required to achieve the equivalent of one ideal stage. It is defined in terms of the height of the packing in the column(H) and N_{stages} as shown in the equation below:

$\text{HETP} = \frac{H}{N_{\text{stages}}}$. (2)

One means of reducing the HETP (i.e., increasing efficiency) is to increase the interfacial area between the liquid and vapor phases. Another method for reducing the HETP is to decrease the time required for molecules to diffuse and equilibrate between the liquid and vapor phases. Because diffusion in liquid is slower than gas phase diffusion, diffusion through the liquid can be the rate-limiting step that slows the approach to equilibrium. Liquid phase diffusion time can be minimized by maintaining well-dispersed high area liquid flow paths throughout the column that are as thin as possible. Distillation devices that seek to maintain these channels at widths below around one millimeter have come to be known as "microchannel distillation" (MCD) devices. The present work is focused on examining the efficiency of two different MCD device concepts and comparing the performance to a more traditional column packing.

MCD has already been applied to various systems to achieve low HETP values. For example, Ziogas et al.[8] used traditional machining and stainless steel layering to achieve an HETP of 1.08 cm in the separation of iso-octane from n-octane. MacInnes et al.[9] used centrifugal forces to achieve an HETP of 0.53 cm in the separation of 2,2-dimethylbutane from 2-methyl-2-butane. For a more comprehensive list, refer to various literature reviews.[10-11]

Additive manufacturing (AM, or 3D printing) is an enabling technology for new distillation column and packing designs. Features can be constructed down to the micrometer scale, and structures can be designed that allow for intimate contact between vapor and liquid phases. Some exploration of AM with distillation has already been performed. Mardani et al.[12] constructed a coil-shaped distillation column using AM and applied it to the separation of cyclohexane from n-hexane. Neukäufer et al.[13] began by designing various structured packings via AM, and then applied some of these[14] to achieve HETP values of 20-25 cm in the separation of cyclohexane and n-heptane. The column used had a height of 2.45 m and a diameter of 50 mm.

Pacific Northwest National Laboratory (PNNL) has previously demonstrated the ability to carry out effective separation in MCD devices using patented microwick technology.[15-18,19-23] This technology employs thin, porous wicks that are ˜100 μm thick, and are alternately stacked between adjacent vapor channels. The liquid in these columns flows by surface tension forces (capillarity), rather than gravity. PNNL first demonstrated distillation with this technology to remove heavy sulfur species from JP8 jet fuel[24] at temperatures above 200°C, with estimated HETP values of 1.8 cm.[25]

One challenge that has been observed with MCD has been the difficulty of maintaining low HETP values at low temperature. For example, Velocys, Inc.[26] applied MCD to the separation of hexane from cyclohexane at temperatures around 70°C and achieved an HETP less than 1 cm. When the same device was applied

to the separation of ethane and ethylene at around -10degC the HETP values doubled. TeGrotenhuis and Powell[18] applied the microwick technique to a horizontal column to separate 3-methylheptane from n-octane at temperatures around 120, with reported HETP values as low as 0.33 cm (N_{stages} ~ 31). When Bottenus et al.[15] used the same device to perform cryogenic distillation of propane and propylene at around -50degC, the HETP value increased by a factor of three to 1.0 cm. A subsequent study by Bottenus et al.[16] reported HETP values as low as 0.42 cm (N_{stages} ~ 60) in the separation of the different carbon isotopes in methane, but performance was still inferior to the theoretical limit of 0.1 cm.

In this work the efficiency of cryogenic air separation is tested using three different small-scale distillation columns. The performance of a random packed column is compared to the performance of two microchannel distillation columns that use thin wicking structures and gas flow channels to achieve process intensification. The HETP values for each column are compared.

Methods

Three different small scale distillation devices were tested: one with traditional random packing, one with microwick plate-type layering (similar to previous PNNL work), and one with a new microchannel porous honeycomb internal structure built via additive manufacturing. All three are shown in Figure 1.

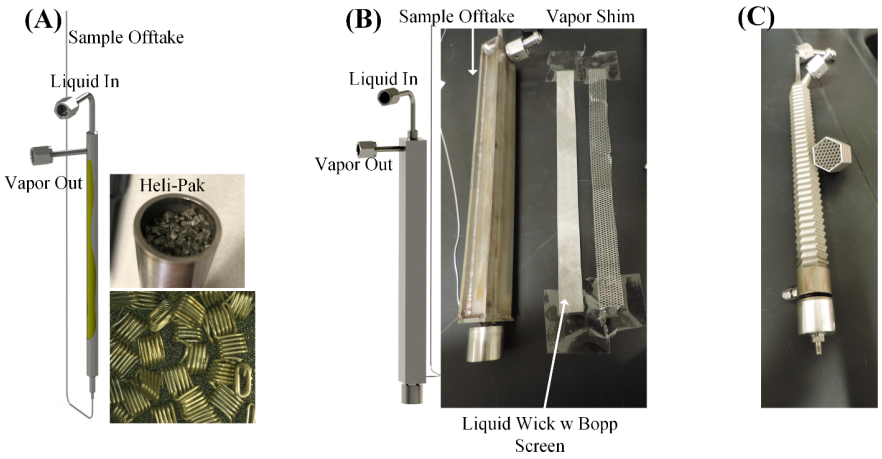

Figure 1. Side-by-side view of the three columns. (A) The traditional packed column with Heli-Pack packing. (B) The plate-type layered (PTL) device alongside sample layers of liquid wick and vapor shim. (C) The additively manufactured porous honeycomb (AMPH) column.

All three columns were built with an active height of 25.4 cm and were operated at 1 atm. Swagelok fittings and additional tubing were welded to each column to provide a liquid inlet, an overhead vapor outlet, and a bottoms liquid outlet. The oxygen-rich reboiler liquid was withdrawn, and the composition determined using a residual gas analyzer. The reboiler liquid level was maintained by monitoring the temperature at different reboiler positions, and reboiler power was supplied via a 20 W electrical heater attached to the outside or the reboiler.

Previous cryogenic experiments with PNNL MCD microwick devices were conducted in an insulated cold box, with the required operating temperatures maintained by periodically spraying liquid nitrogen inside the box. This required significant quantities of liquid nitrogen; one 24-hour experiment consumed multiple 180 L dewars. It also made simultaneous control of both the cold box temperature and the condenser duty difficult. To avoid these difficulties, in the present work each distillation system was placed inside a vacuum can, which provides more efficient insulation. A Stirling Cryocooler (SunPower CryoTel® GT) was used as a cooling source, rather than liquid nitrogen.

Traditional Random Packing (TRP)

The traditional packed column was a vertical cylinder with an inside diameter of 1.09 cm. It was filled with stainless steel Heli-Pak packing distributed randomly. Liquid entered near the top of the column and flowed downward through the packing. This TRP device is representative of a typical small, packed column and served as a benchmark against which to compare the other two columns.

Plate-Type Layering (PTL)

The PTL column was built in the shape of a rectangular prism, with inner dimensions of 1.9 cm x 1.9 cm. It used an arrangement similar to that of the previous PNNL microwick device; however, unlike previous PNNL microwick experiments this device was operated in a vertical, as opposed to horizontal, direction. Internally, it was configured with a specific arrangement of three different types of materials: thicker vapor channels (0.05 cm), thinner liquid wicks (0.01 cm), and fine screens (˜38 μm). The vapor channels and liquid wicks were expanded metal screens, and the materials were layered as shown in Figure 2, with each layer extending from the top to the bottom of the column.

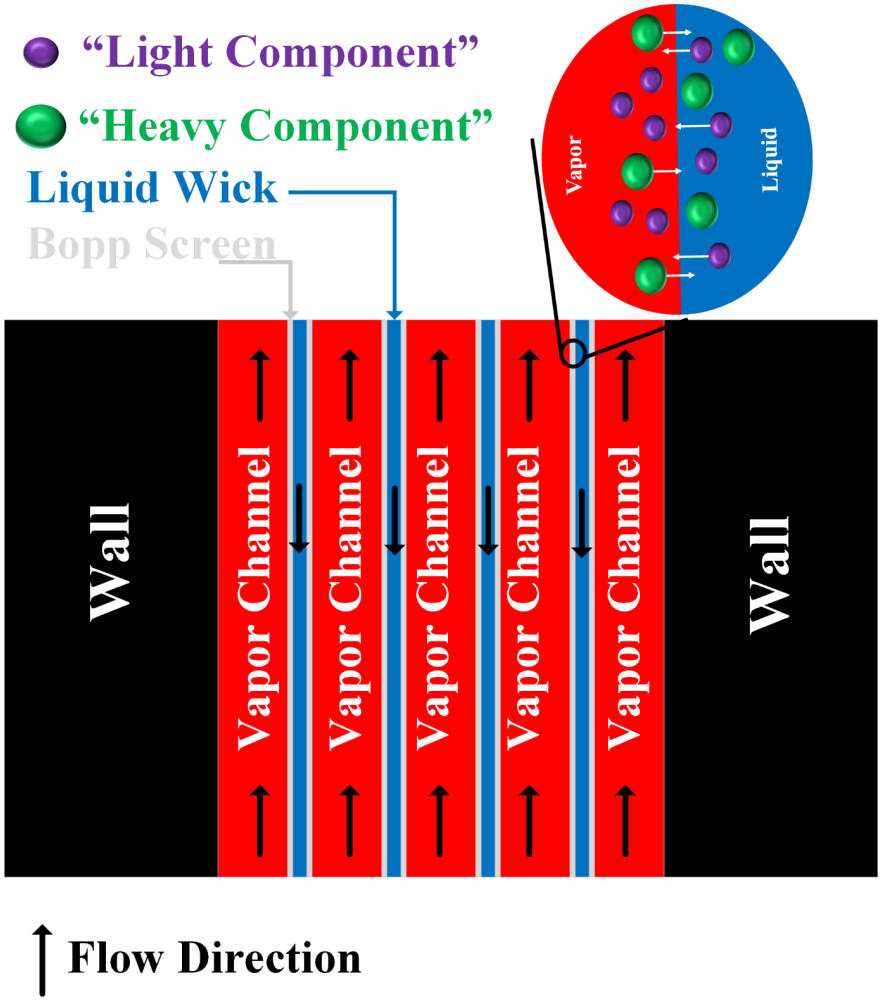

Figure 2 . Sample layer arrangement in the plate-type MCD.

The layers followed a vapor-liquid-vapor pattern, with each liquid wick sandwiched between two fine screens. The overall arrangement included 29 vapor channels, 28 liquid wicks, and 56 fine screens. The vapor channels were filled with stainless-steel mesh with larger openings to provide a non-wicking region for vapor flow. The fine screens were Bopp SDS PLUS 53/24 woven mesh and served to prevent intrusion of the vapor into the liquid wicks. The vapor and liquid wicking screens were pressed together into the rectangular housing, and the side and ends of the device were sealed by welding. A small section at the bottom of the column was left empty for the bottoms liquid to accumulate.

Additively-Manufactured Porous Honeycomb (AMPH)

The third device is new to this work and is referred to as the additively-manufactured porous honeycomb (AMPH) column. Its structure is shown in Figure 3.

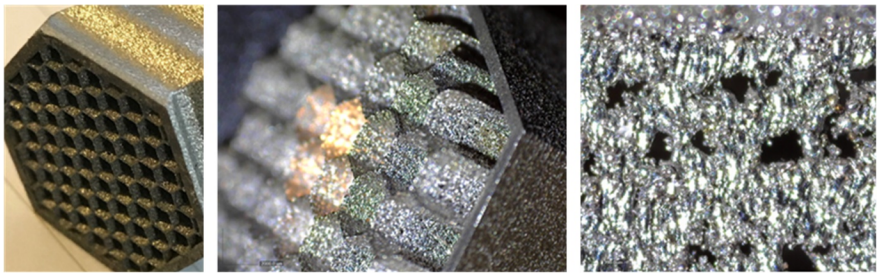

Figure 3 . Images of the AMPH device at 1x (left), 20x (center), and 235x (right) magnification. The width of the octagonal device is 27 mm. The column is comprised of an internal solid framework surrounded by a solid outer shell. The framework is built of porous walls that are ˜150 µm thick. The framework has a hexagonal honeycomb-like structure, and in the vertical direction it follows an undulating pattern to minimize the possibility of liquid droplets falling through the device without interacting with the wicking structures. This undulation generates the wave-like surface of the outer shell (Figure 1 (C)).

The column was first designed in CAD software (SolidWorks 2019) and then manufactured via an additive printing process that employs direct metal laser sintering: a laser melts metal powder one layer at a time, gradually building on previous layers until the entire structure is completed. The internal honeycomb is a high-porosity metal scaffold created by scanning the laser quickly and at a heat intensity that is too low to completely melt the metal powder. The solid outer shell is made with laser power and scan settings that produce high-density, non-permeable metal. The manufacturing was performed by i3DMFG^{TM} and printed with nickel-based Inconel 625 using custom print settings.

Distillation System

The distillation system consists of a microchannel recuperator to precool the incoming air, a custom condenser that attaches to the cold head of the stirling cryocooler, the distillation column, and a vacuum can that contains these components and provide thermal insulation. The same vacuum can, condenser, and recuperator were used for all experiments, with the distillation column being changed for each set of tests. The system configuration is shown in Figure 4.

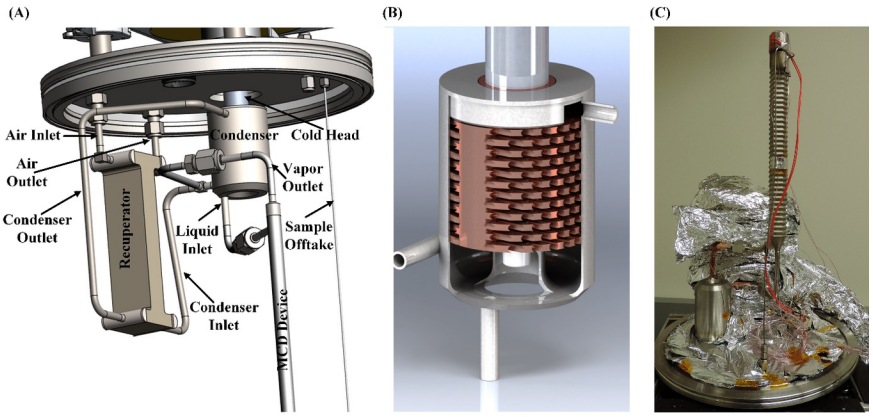

Figure 4. (A) CAD model of the portion of the MCD system contained within the vacuum can. (B) CAD model of the custom-built condenser. (C) Image of the MCD system with the vacuum can lid lying on a flat surface, when running the orientation is inverted with the column hanging down from the lid.

The incoming air is dried, and CO_2 removed using adsorption cartridges containing 13X molecular sieve material. Mass flow controllers are used to control the flowrate of the incoming air and the bottoms stream exiting the reboiler. The condenser—shown in Figure 4(B)—contains a heat transfer surface custom-machined from a copper block contained in a stainless-steel housing. It was situated around and attached to the cold head of the cryocooler, a Sunpower CryoTel® GT 16 W unit. During testing, the cryocooler cold head operated around 77 K (-196degC), at which temperature it provided 16 W of lift (per manufacturer specifications). The feed entered the bottom of the condenser and the nitrogen rich gas exited to top of the condenser.

To provide thermal insulation, the heat exchanger, column, and condenser were all enclosed within the vacuum can. The pressure inside the can was maintained below 10^{-4} torr, and the pieces of equipment inside the vacuum can were each wrapped in 5-10 layers of 500 DM cryogenic laminate (multi-layer insulation). Swagelok and flange fittings were used for all connections. Type K thermocouples were placed on the inlet and outlet of the various components to monitor temperatures throughout the system. Opto 22 software was used to monitor the temperatures, flowrates, and pressures inside the vacuum can, as well as the pressure of the process fluid in the distillation system. The power inputs to the cryocooler and the reboiler were also modulated using Opto 22. A vacuum pump was connected to the reboiler for continuous removal of liquid. The flow rate was measured by a mass flow controller and verified with a Mesa Labs Definer 220-L DryCal. A small sample of the reboiler vapor was periodically withdrawn and sent to the Dycor residual gas analyzer for compositional analysis. The residual gas analyzer pulls samples at vacuum pressures, so the gas was assumed to be ideal. Consequently, the total pressure P was assumed to equal the sum of the individual species partial pressures P_i, and the species mole fractions y_i were assumed to be directly proportional to the species partial pressures (i.e.,$y_i = \frac{P_i}{P}$).

Process Flow

Atmospheric air was first processed through the adsorption cartridges. The CO_2-free dry air is then precooled in the recuperator inside the vacuum can. The cooled dry air then flows into the condenser and was partially condensed. The uncondensed vapor—mostly nitrogen—flows back through the heat exchanger. The condensed liquid collects in the bottom of the condenser and then flows into the column, passes down through the column, and is eventually collected in the reboiler. Along the way, it interacts continuously with the upward moving vapor produced in the reboiler. The less volatile components—primarily oxygen and argon but also other heavy components such as xenon—became concentrated in the liquid, while the more volatile nitrogen becomes concentrated in the vapor. A portion of the liquid in the reboiler is periodically withdrawn and sampled.

Operation

During startup, the reboiler is turned off while waiting for the system to cool down to operating temperatures. This cooling process took a couple of hours. All three columns were tested under similar conditions with maximum reflux to compare separation efficiency. For these tests, the feed air flow rate was fixed at 1 SLM (standard volumetric flow) and the flow rate of the bottoms liquid product was kept below 0.01 SLM (also standard volumetric flow). The AMPH device was also tested to determine the maximum flow of oxygen-rich product (minimum mole fraction 0.90) that could be produced by the equipment. For these tests the feed air flow rate was fixed at 5 SLM and the bottoms liquid product flow was adjusted from 0.140 to 0.400 SLM in increments of 0.054 SLM.

Modeling

The MCD system was modeled using process simulation software, the flowsheet for which is shown in Figure 5**.** This is a very simple model, consisting of only a heat exchanger to model the recuperator and a distillation column to model the MCD column.

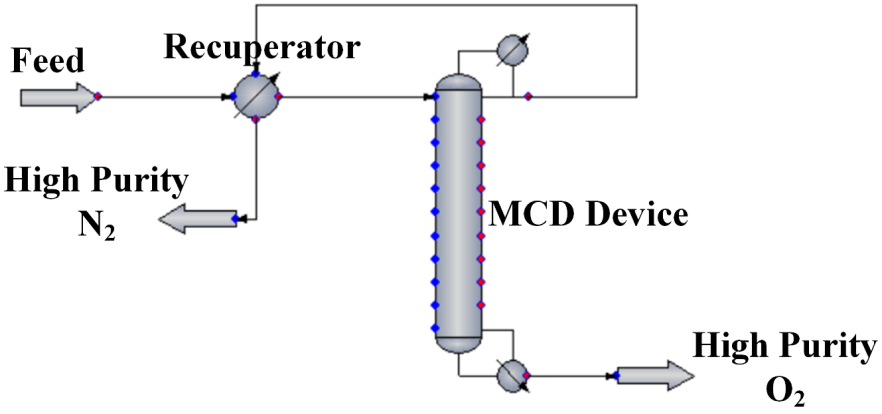

Figure 5. Flowsheet for the process simulation model used to simulate the MCD system.

For all model runs, the feed stream (stream 1 in Figure 5) was configured with a temperature of 25°C, a pressure of 1 atm, and a molar fractional composition representative of common air (0.78 N_2, 0.21 O_2, 0.01 Ar). This stream was also configured to enter the column at stage 1. The temperature of the nitrogen-rich outlet stream from the heat exchanger (stream 5) was set to -2degC. This value was based on measurements from the experiments and indicated a 27degC difference between the hot side inlet and cold side outlet for the exchanger.

To ensure the model results were not dependent on any single simulator, the model was executed in three different software packages: CHEMCAD (v7.1.6), Aspen HYSYS V11, and DWSIM (v6.7.1). The Peng-Robinson equation of state (EOS) was used for all thermodynamic calculations.

To model the separation efficiency (which, again, was focused on comparing the separation efficiency of the three different columns), the standard volumetric flow rates of the feed (stream 1) and bottoms liquid product (stream 3) were set to 1.0 and 0.01 SLM, respectively, and the condenser duty was fixed at -16 W. The number of stages in the model column was adjusted from 2 to 20, and the composition of the bottoms liquid product was recorded for each stage. The number of theoretical stages of separation achieved by each MCD column was then determined by matching the composition measured in the experiments to that of the model.

To model the maximum oxygen production the standard vapor volumetric flow of the feed (stream 1) was increased to 5 SLM, the number of column stages was fixed at 8, the condenser duty was initially kept at

-16 W, and the standard vapor volumetric flow of the bottoms liquid product (stream 5) was incremented from 0.1 SLM until the oxygen mole fraction in this stream fell below 0.90.

Results and Discussion

Before discussing the performance of the three devices, a few observations are of note. First, previous PNNL MCD microwick devices[15, 16] had been operated in the horizontal direction, with liquid flow manipulated via siphons. Balancing all process parameters to achieve steady-state operation with these devices had required significant effort. Operating the PTL column vertically in this work proved to be more straightforward, with no additional equipment required to promote fluid flow. While this is an important improvement, it does come at one cost: the flow rate at low flows cannot be controlled as precisely as with the horizontal device. Where very low flows are important, future work with AMPH columns could include both horizontal structures to aid in separation efficiency and vertical features to aid in operation, a sort of hybrid between gravity-driven flow and capillary flow from wicking.

Second, the use of a vacuum can and a cryocooler—rather than a cold box with liquid nitrogen—led to a significant reduction in both heat losses and temperature fluctuations. This made the system more robust and easier to operate than previous systems.

Separation efficiency tests

Figure 6 shows a sample of the experimental results during separation efficiency tests for the AMPH column. Note that the pressure values show the partial pressures measured in the residual gas analyzer that operates at vacuum conditions. These partial pressure measurements provide information about the relative amount of each species exiting the reboiler.

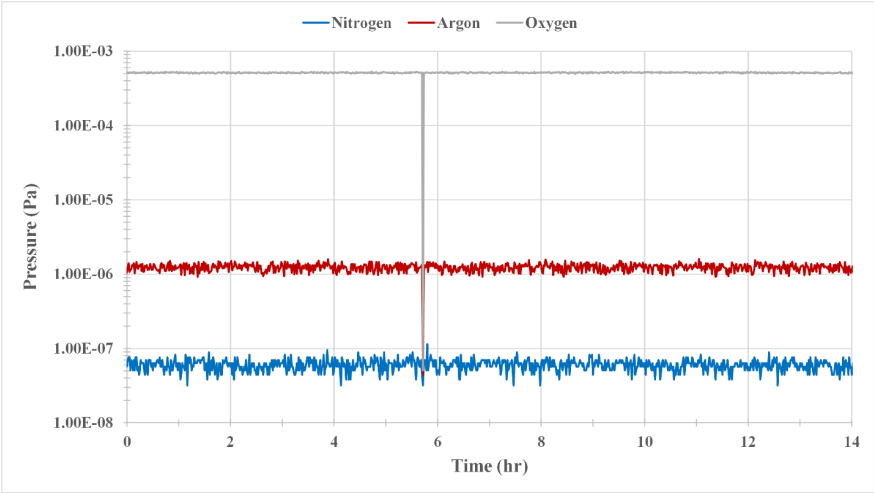

Figure 6. Sample measured data for the bottoms product of the AMPH column during steady state operation, with the partial pressure of each component shown as a function of time. The momentary drop in values at around 6 hours was the result of a temporary instrument failure.

In this plot the average partial pressures for oxygen and argon are 5.2[?]10^{-4} and 1.3[?]10^{-3} Pa, respectively, corresponding to mole fractions of 0.9975 and 0.0025. Apart from a momentary instrument failure shortly after the 6-hour mark, the measurements showed little variation. For example, the standard deviation for

the argon partial pressure over the final 4 hours is 1.3[?]10^{-7} Pa. Adding one standard deviation in either direction of the mean gives an estimate of 0.0022 to 0.0027 for the argon mole fraction.

The plot also shows that the nitrogen partial pressure remained low throughout the process, indicating that virtually all the nitrogen in the feed was exiting in the overhead vapor. Values for other trace components in air (e.g., neon, krypton, and xenon) were measured as well, but their values all remained below those of nitrogen and are not shown here. To collect these trace components, the reboiler flow would need to be turned off to allow these noble gases to accumulate.

Comparable measurements for the PTL column showed an argon mole fraction of 0.0068 ($\pm$ 0.0001), with just a small amount of nitrogen (0.0004 $\pm$ 10^{-5}). Measurements for the TRP column showed mole fractions of around 0.0090 for both argon and nitrogen.

Results for the three different simulation models are shown in Figure 7. These are sufficiently similar to allow a determination of the number of ideal stages equivalent for all three. Thus, the conclusions below are not dependent on a single simulator.

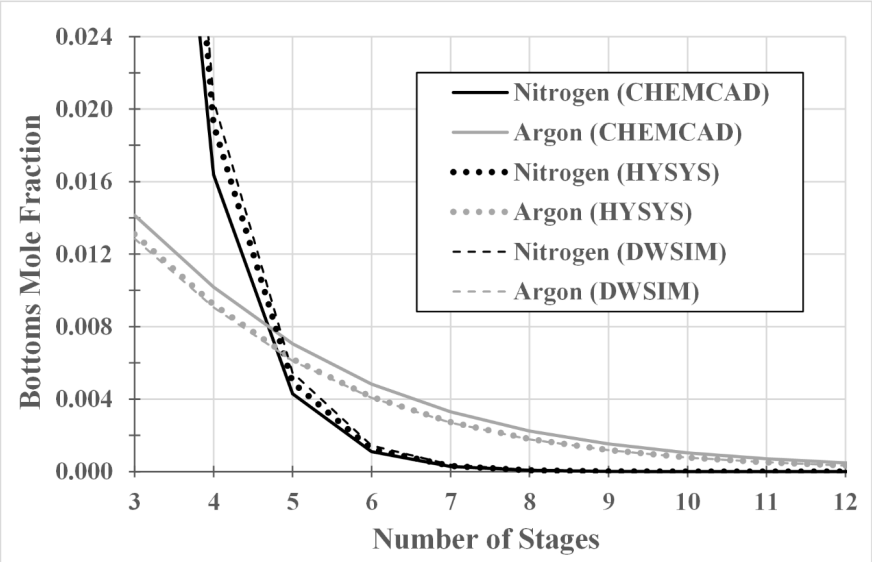

Figure 7 . Results for the CHEMCAD, Aspen HYSYS, and DWSIM simulation models. All three agree within reasonable accuracy.

Figure 8 compares the results for each column with the ideal stage model. For the TPR column, both the argon and nitrogen values match the model at around 4.5 stages. For the PTL column the argon and nitrogen values match the model at around 5 and 7 stages, respectively, while for the AMPH column both argon and nitrogen match at around 8 stages.

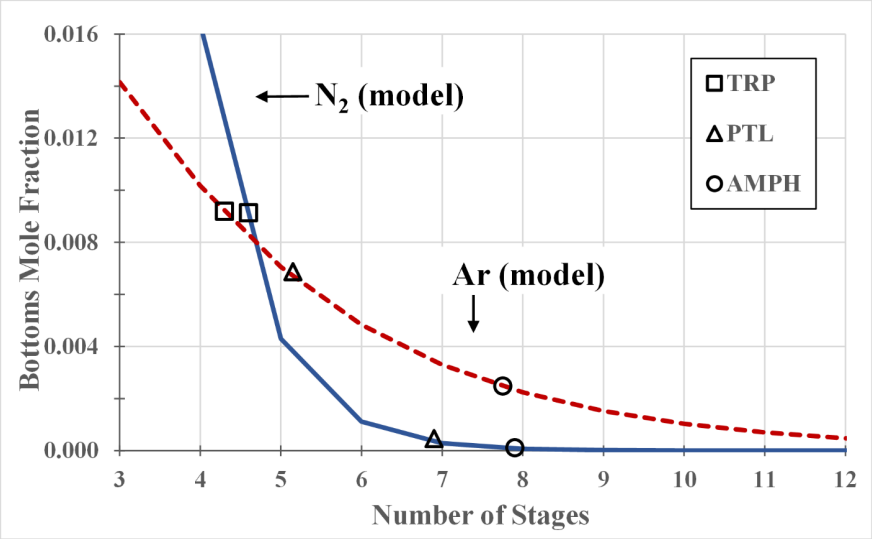

Figure 8 . Results for the bottoms liquid composition of the three MCD columns. The solid and dashed lines indicate values from the ideal stage model for nitrogen and argon, respectively, while points indicate the experimentally measured values for each respective column. The number of stages includes the condenser and reboiler, each of which represents one ideal stage.

These results are summarized in Table 1. Note that the HETP values referenced previously in this work apply to the separation of binary mixtures, where a single value is sufficient to describe the separation of the two components. Air, however, is a mixture of more than just two components, so the results are presented here in terms of separate HETP values for nitrogen and argon.

Table 1. Results for each MCD column. HETP values are relative to a column height of 25.4 cm, and are thus in units of cm.

	Nitrogen	**Nitrogen**	**Nitrogen**	**Argon**	**Argon**	**Argon**
MCD column	**y**	**N_{stages}**	HETP	**y**	**N_{stages}**	HETP
TRP	0.0091	4.6	5.5	0.0092	4.3	5.9
PTL	0.0005	6.9	3.7	0.0071	5.2	4.9
AMPH	0.0001	7.9	3.2	0.0025	7.8	3.3

The HETP values for the TRP column are consistent with a previous study[27] that used similar random packing for nitrogen-argon separation. HETP values for the PTL column are lower, while those for the AMPH column are the lowest (3.2 cm for nitrogen, 3.3 cm for argon). Thus, the AMPH column is the most effective of the three. This increase in separation efficiency with the same column height is an example of process intensification through improvement of the gas liquid interface in the column.

Figure 9 shows how the result for the AMPH column (3.2 cm) is consistent with HETP values from previous PNNL MCD studies. In general, HETP values increase with mass flux.

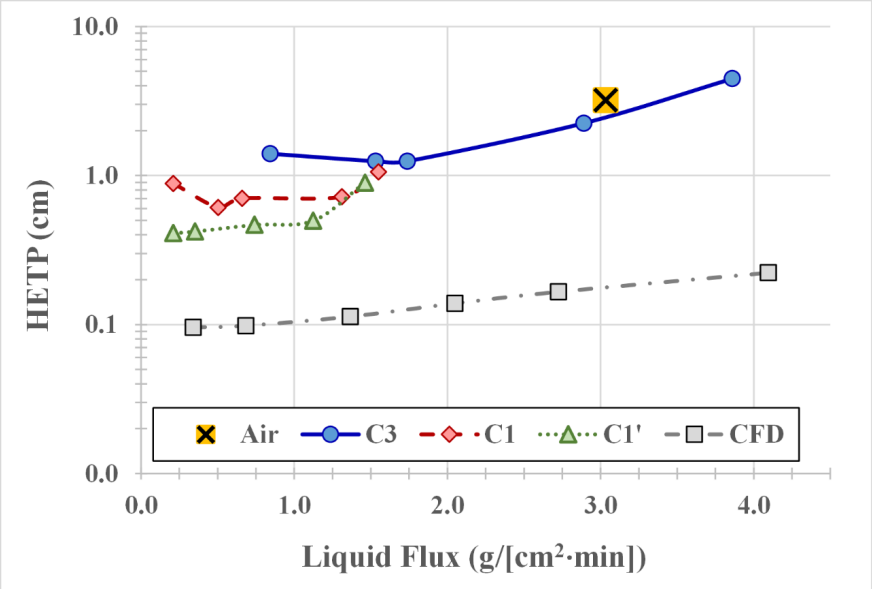

Figure 9. A comparison of the HETP values obtained from various PNNL MCD devices, each as a function of mass flux. Note the logarithmic scale for the HETP values. The data for this figure is taken from a previous publication[17], with one point (Air) from the current work added for reference. C3 refers to propane/propylene separation with a 10.2 cm device; C1 and C1' are for methane isotope separation with a 10.2 and 25.4 cm device, respectively; and CFD is for a computational fluid dynamics simulation based on the propane/propylene separation in the 10.2 cm long PTL device with liquid wicks and vapor channels with heights of 100 μm and 500 μm, respectively.

Reboiler outlet flow testing

Figure 10 shows the experimental measurements and model predictions for testing to determine the maximum reboiler outlet flow. The experimental values show that the AMPH column used in this work is capable of producing up to about 0.4 SLM of product containing at least 90% oxygen.

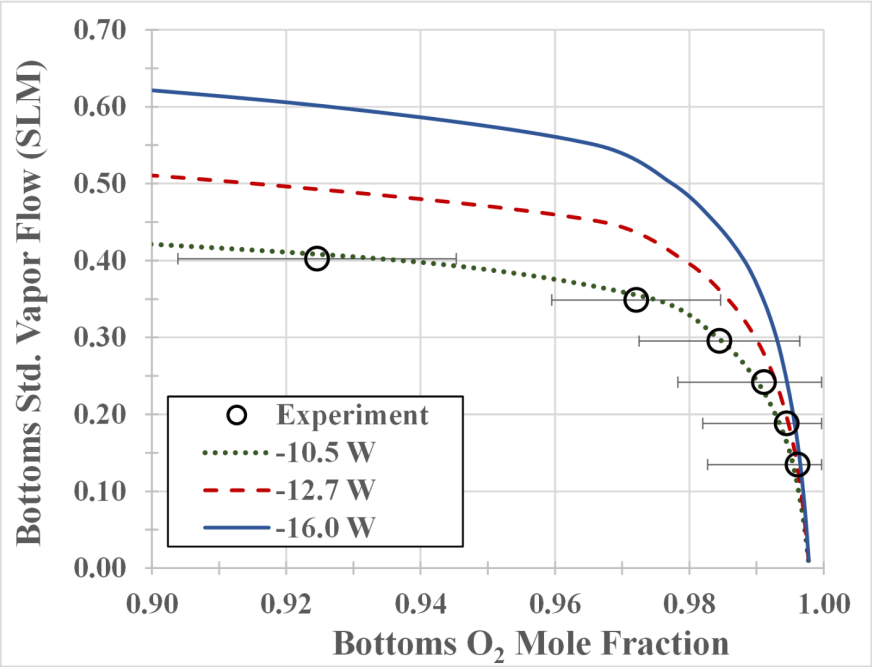

Figure 10. Results from reboiler outlet flow tests. Circles represent experimental measurements, with solid horizontal error bars indicating one standard deviation in either direction. The lines indicate values from the ideal stage model at three different condenser duties.

Comparing the experimental measurements to the base model predictions (condenser duty -16 W), noticeable deviation is evident at bottoms liquid flow rates above about 0.20 SLM. One source of this discrepancy could be the that the cryocooler was not actually providing the full advertised duty provided by the manufacturer. Accordingly, a separate experiment was performed to measure the cryocooler duty.

A 5 Ω resistor was mounted to the cryocooler and 9 different voltages between 6 and 10 V were applied through the resistor. At each voltage the cryocooler temperature was measured via a thermocouple, and once the temperature stabilized, the current was measured. The results are shown in Figure 11, with power (P_W) calculated from the current (I) and resistance (R) via$P_W = I^2R$.

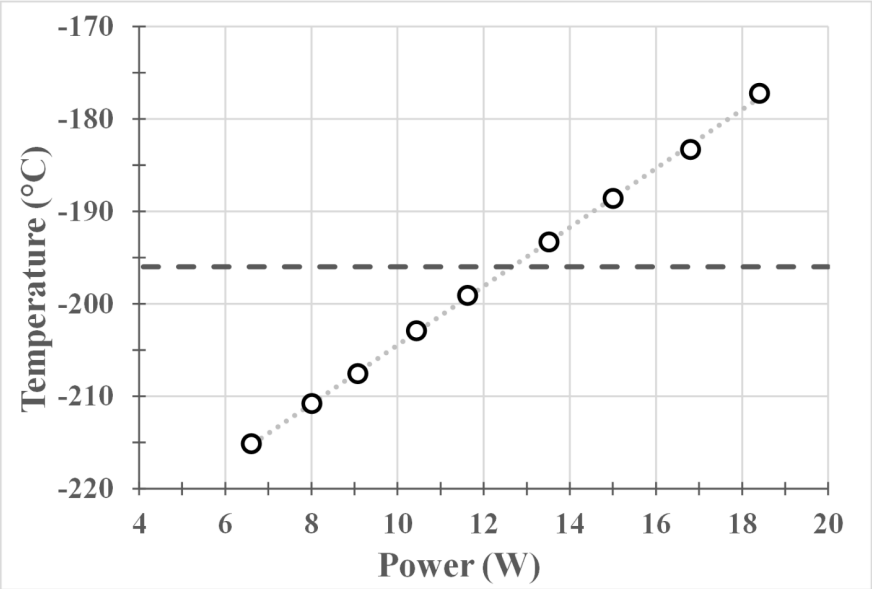

Figure 11. Performance data for the cryocooler. Circles indicate the experimental data, the dotted line shows a linear fit to the data, and the dashed line indicates the operating temperature for the cryocooler in the MCD system.

These results suggest that the cryocooler was providing about 12.7 W of duty to the condenser during MCD operation, which is 3.3 W less than the manufacturer's specifications. Reducing the condenser duty in the model to 12.7 W improves the fit with the experimental data, but there is still some disagreement. Reducing the duty in the model to 10.5 W allows the model to agree closely with the data. This additional 2.2 W difference is likely the result of parasitic heat losses (i.e., losses that result from imperfect insulation of the process).

One note about these results should be emphasized. The condenser duty in the model has only minimal impact on composition when the bottoms flow rate is small and the boil up ratio is high. Since the modeling and experiments used to determine column efficiency was performed at small bottoms flow rates, this finding about the actual condenser duty had no impact on the determination of the HETP values for each column.

Conclusion and Outlook

The work described here demonstrates that, relative to traditional random packing, the separation efficiency of oxygen from air in an MCD column can be greatly enhanced by using a custom AMPH internal structure. This enhanced efficiency results from the porous liquid wicking structures present in the AMPH column itself, not to anything unique to air separation. Accordingly, this approach can reasonably be expected to improve efficiency in other types of distillation systems as well. This enhanced efficiency is an enabling technology for small scale air separations including the collection of xenon from the atmosphere.

AM allows internal structures to be constructed that are not available via traditional manufacturing techniques. Future work in distillation could continue to explore other structural changes to improve mass transfer. Further, the improvement observed here suggests that AM could be applied to other processes for similar improvement. For example, it is possible that the efficiency and/or selectivity of an adsorption process could be improved by controlling the microstructure of the adsorbent via AM. Similarly, AM could be used to create heat exchangers with internal flow structures that optimize heat transfer in ways not heretofore possible.

The principles that allow the AMPH MCD column to improve separation efficiency should scale up to larger distillation systems, but current direct metal laser sintering equipment constrains the maximum part size that can be fabricated. For example, the i3DMFG^{TM} EOS® M400.4 platform used in this work is a 40x40x40 cm cube, so the part must fit within those dimensions. Also, in a distillation column the fluid entering the column must be properly distributed across its entire width. In columns with small widths—such as those tested in this work—this is straightforward and requires no special design, but with a larger device this would likely require a specialized header to distribute uniform liquid flow to the wicking structures.

Acknowledgements

This research was funded by the National Nuclear Security Administration, Defense Nuclear Nonproliferation Research and Development (NNSA DNN R&D). Support was also provided by the DOE Hydrogen and Fuel Cell Technology Office, and the DOE Office of Fossil Energy. The authors acknowledge important interdisciplinary collaboration with scientist and engineers from LANL, LLNL, MSTS, PNNL, and SNL. PNNL is operated by Battelle Memorial Institute for the U.S Department of Energy (DOE under Contract No. DE-AC05-76RL01830. Thanks also go to Michael Ripplinger, William Sliger, Nathan Canfield and Lance Hubbard of PNNL for their contributions to the project.

Notation

H height of the packed column, cm

HETP height equivalent of a theoretical plate, cm

I current, A

N_{stages} number of ideal stages

N_{trays} number of column trays

P total system pressure, Pa

P_i partial pressure of species i, Pa

P_w power, W

R resistance, ohms

SLM standard liter per minute, L/min

y_i mole fraction of species i

Abbreviations

AMPH additively manufactured porous honeycomb

Ar Argon

CAD computer-aided design

CO_2 carbon dioxide

DOE Department of Energy

DNN Defense Nuclear Nonproliferation

EOS equation of state

LANL Los Alamos National Laboratory

LLNL Lawrence Livermore National Laboratory

MCD microchannel distillation

MSTS Mission Support and Test Services

N_2 Nitrogen

NNSA National Nuclear Security Administration

O_2 Oxygen

PNNL Pacific Northwest National Laboratory

PTL plate-type layered

R&D Research and Development

SNL Sandia National Laboratory

Greek Letters

η column efficiency

Ω resistance, ohms

Literature Cited

1. Avasthi A, Bowyer TW, Bray C, et al. Kiloton-scale xenon detectors for neutrinoless double beta decay and other new physics searches.*Physical Review D* . 12/20/2021 2021;104(11):112007. doi:10.1103/PhysRevD.104.112007

2. Bowyer TW. A Review of Global Radioxenon Background Research and Issues. *Pure and Applied Geophysics* . 2021/07/01 2021;178(7):2665-2675. doi:10.1007/s00024-020-02440-0

3. Hashim SS, Mohamed AR, Bhatia S. Oxygen separation from air using ceramic-based membrane technology for sustainable fuel production and power generation. *Renewable and Sustainable Energy Reviews* . 2011;15(2):1284-1293. doi:https://doi.org/10.1016/j.rser.2010.10.002

4. Hinchliffe AB, Porter KE. A Comparison of Membrane Separation and Distillation. *Chemical Engineering Research and Design* . 2000;78(2):255-268. doi:https://doi.org/10.1205/026387600527121

5. Hu T, Zhou H, Peng H, Jiang H. Nitrogen Production by Efficiently Removing Oxygen From Air Using a Perovskite Hollow-Fiber Membrane With Porous Catalytic Layer. Original Research. *Frontiers in Chemistry* . 2018-August-06 2018;6(329)doi:10.3389/fchem.2018.00329

6. Koros WJ, Mahajan R. Pushing the limits on possibilities for large scale gas separation: which strategies? *Journal of Membrane Science* . 2000/08/10/ 2000;175(2):181-196. doi:https://doi.org/10.1016/S0376-7388(00)00418-X

7. Yoshida S, Ogawa N, Kamioka K, Hirano S, Mori T. Study of Zeolite Molecular Sieves for Production of Oxygen by Using Pressure Swing Adsorption. *Adsorption* . 1999/01/01 1999;5(1):57-61. doi:10.1023/A:1026402425399

8. Ziogas A, Cominos V, Kolb G, Kost HJ, Werner B, Hessel V. Development of a Microrectification Apparatus for Analytical and Preparative Applications. *Chem Eng Technol* . Jan 2012;35(1):58-71. doi:10.1002/ceat.201100505.

9. MacInnes JM, Zambri MKS. Hydrodynamic characteristics of a rotating spiral fluid-phase contactor. *Chem Eng Sci* . Apr 14 2015;126:427-439. doi:https://doi.org/10.1016/j.ces.2014.12.036.

10. Lam KF, Sorensen E, Gavriilidis A. Review on gas-liquid separations in microchannel devices. *Chem Eng Res Des* . Oct 2013;91(10):1941-1953. doi:https://doi.org/10.1016/j.cherd.2013.07.031.

11. Yang RJ, Liu CC, Wang YN, Hou HH, Fu LM. A comprehensive review of micro-distillation methods. *Chem Eng J* . Apr 1 2017;313:1509-1520. doi:10.1016/j.cej.2016.11.041.

12. Mardani S, Ojala LS, Uusi-Kyyny P, Alopaeus V. Development of a unique modular distillation column using 3D printing. *Chemical Engineering and Processing - Process Intensification* . 2016/11/01/ 2016;109:136-148. doi:https://doi.org/10.1016/j.cep.2016.09.001.

13. Neukäufer J, Hanusch F, Kutscherauer M, Rehfeldt S, Klein H, Grützner T. Methodology for the Development of Additively Manufactured Packings in Thermal Separation Technology. *Chem Eng Technol* . 2019;42(9):1970-1977. doi:https://doi.org/10.1002/ceat.201900220.

14. Neukäufer J, Sarajlic N, Klein H, et al. Flexible distillation test rig on a laboratory scale for characterization of additively manufactured packings. *Aiche Journal* . 2021;doi:10.1002/aic.17381.

15. Bottenus D, Caldwell D, Fischer C, et al. Process intensification of distillation using a microwick technology to demonstrate separation of propane and propylene. *Aiche Journal* . 2018;64:3690-3699. doi:10.1002/aic.16325.

16. Bottenus D, Veldman T, Caldwell D, et al. Isotope Enrichment of 13C from Methane in Microchannel Distillation Devices at Cryogenic Temperatures. *To Be Submitted* . 2022:XXX-XXX.

17. TeGrotenhuis W, Bottenus D, Hoppe E, Humble P, Lucke R, Powell M.*Isotope Enrichment Using Microchannel Distillation Technology* . 2018.

18. TeGrotenhuis WE, Powell MR. Packing Structure Capable of Sub-Centimeter HETP for High Purity Distillation of Low Relative Volatility Compounds. American Institute of Chemical Engineers Conference Proceedings; April 3, 2012.

19. TeGrotenhuis WE, Wegeng RS, Whyatt GA, Stenkamp VS, Gaulitz PA, inventors; Battelle Memorial Institute, assignee. Microsystem capillaray separations. United States patent 6,666,909. 2003.

20. Tegrotenhuis WE, Stenkamp VS, inventors; Battelle Memorial Institute, USA . assignee. Conditions for fluid separations in microchannels, capillary-driven fluid separations, and laminated devices capable of separating fluids. United States patent application US-1138601-A. 2002.

21. TeGrotenhuis WE, Stenkamp VS, inventors; Battelle Memorial Institute, assignee. Methods for fluid separations, and devices capable of separating fluids. United States patent 7,051,540. 2006.

22. TeGrotenhuis WE, Stenkamp VS, inventors; Improved conditions for fluid separations in microchannels, capillary-driven fluid separations, and laminated devices capable of separating fluid. patent US Patent 6,875,247. 2005.

23. Stenkamp VS, TeGrotenhuis WE, Wegeng RS, inventors; Battelle Memorial Institute, assignee. Mixing in wicking structures and the use of enhanced mixing within wicks in microchannel devices. United States patent 7,540,475. 2009.

24. Huang XW, King DA, Zheng F, et al. Hydrodesulfurization of JP-8 fuel and its microchannel distillate using steam reformate. *Catal Today* . Jul 31 2008;136(3-4):291-300. doi:10.1016/J.CATTOD.2008.01.011.

25. Sundberg A, Uusi-Kyyny P, Alopaeus V. Novel micro-distillation column for process development. *Chem Eng Res Des* . May 2009;87(5a):705-710. doi:10.1016/j.cherd.2008.09.011.

26. Hickey T. Advanced Distillation Final Report. Velocys, Inc. http://www.osti.gov/scitech/servlets/purl/1000368

27. Yamanishi T, Kinoshita M. Preliminary Experimental-Study for Cryogenic Distillation Column with Small Inner Diameter, .2. *J Nucl Sci Technol* . 1984;21(11):853-861. doi:10.1080/18811248.1984.9731124.

Hosted file

`Table 1.docx` available at https://authorea.com/users/472143/articles/563190-additively-manufactured-cryogenic-microchannel-distillation-device-for-air-separation